MATERIALS CHEMISTRY FRONTIERS

RESEARCH ARTICLE

View Article Online
View Journal





Cite this: DOI: 10.1039/d2qm00106c

# Orthogonal redox and optical stimuli can induce independent responses for catechol-chitosan films†

Zhiling Zhao, [ab] Eunkyoung Kim, [ab] Chen-Yu Chen, [c] John R. Rzasa, [b] Qian Zhang, [d] Jinyang Li, [c] Yang Tao, [c] William E. Bentley, [abc] Jean-Philip Lumb, [e] Bern Kohler [f] and Gregory F. Payne *[ab]

Received 7th February 2022,
Accepted 5th April 2022

DOI: 10.1039/d2qm00106c

rsc.li/frontiers-materials

Catechol-based materials possess diverse properties that are especially well-suitable for redox-based bioelectronics. Previous top-down, systems-level property measurements have shown that catechol-polysaccharide films (*e.g.*, catechol-chitosan films) are redox-active and allow electrons to flow through the catechol/quinone moieties *via* thermodynamically-constrained redox reactions. Here, we report that catechol-chitosan films are also photothermally responsive and enable near infrared (NIR) radiation to be transduced into heat. When we simultaneously stimulated catechol-chitosan films with NIR and redox inputs, times-series measurements showed that the responses were reversible and largely independent. Fundamentally, these top-down measurements suggest that the flow of energy through catechol-based materials *via* the redox-based molecular modality and the electromagnetic-based optical modality can be independent. Practically, this work further illustrates the potential of catecholic materials for bridging bio-device communication because it enables communication through both short-range redox modalities and long-range electromagnetic modalities.

## Introduction

Catecholic materials offer diverse functional properties in biology (*e.g.*, melanins[1]) and technology (*e.g.*, polydopamines[2–4]). Recently, various natural and synthetically-fabricated catechol-based materials have been shown by top-down systems-level measurements to be redox-active and can be repeatedly oxidized and reduced.[5–9] Some of the functional properties of catechol materials have been shown to depend on their redox-activities (*i.e.*, reactive oxygen species generation[10–13] and radical scavenging[14–16]) or their redox-state (*e.g.*, metal chelation[17,18]). However for other properties, an association with redox-activity is less clear.[19–21] Specifically, various catecholic materials show strong photothermal heating upon near infrared (NIR) irradiation,[22–28] yet it is not always clear if the responses to optical and redox stimuli are independent. Scheme 1 illustrates the NIR-induced excitation of electrons and the redox-based transfer of electrons, and the question in this study is whether the response to inputs from these orthogonal modalities can be independent.

Our focus is redox-active catechol-polysaccharide films that are being investigated for applications in molecular electronics (*e.g.*, molecular memory[29,30]) and biomaterials (*e.g.*, antimicrobial dressings[11]). Here, we report that top-down property measurements indicate that catechol-chitosan films possess photothermal properties and the response of these films to simultaneous redox and NIR stimulation appears to be independent. As discussed, we believe the independence of the opto-redox responses suggests that catechol moieties can facilitate biodevice communication by enabling the flow of energy and information through orthogonal information processing modalities.

## Results and discussion

To detect photothermal effects, we first cast chitosan films on glass slides and patterned these transparent chitosan films with catechol dots (2 mm diameter) as illustrated in Fig. 1a.

[a] Institute for Bioscience and Biotechnology Research, University of Maryland, College Park, Maryland 20742, USA. E-mail: gpayne@umd.edu
[b] Robert E. Fischell Institute for Biomedical Devices, University of Maryland, College Park, Maryland 20742, USA
[c] Fischell Department of Bioengineering, University of Maryland, College Park, Maryland 20742, USA
[d] Department of Chemistry and Biochemistry, University of Maryland, College Park, Maryland 20742, USA
[e] Department of Chemistry, McGill University, Montreal, Quebec H3A 0B8, Canada
[f] Department of Chemistry and Biochemistry, The Ohio State University, Columbus, Ohio 43210, USA

† Electronic supplementary information (ESI) available. See DOI: https://doi.org/10.1039/d2qm00106c

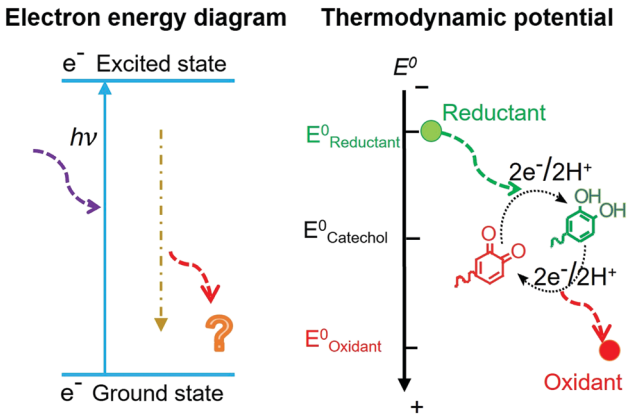


Scheme 1 Electrons can be excited by electromagnetic energy and can be transferred through energetically favorable molecular-based reduction–oxidation (redox) reactions.

These dots were fabricated by immersing the films in a catechol solution (10 mM in 0.1 M, pH 7.0 phosphate buffer) positioning an electrode "pen" above the film and inducing oxidative grafting by applying an anodic voltage (+0.5 V *vs.* Ag|AgCl for varying times up to 10 minutes) to generate patterns with varying extents of modification as measured by $Q_{fab}$ $(Q_{fab} = \int i dt)$.[29] Fig. S1 and the associated text of the ESI† provide a brief summary of chemical evidence for the oxidative grafting of catechol to chitosan films.[31,32] These films were rinsed, air-dried, wet with a small amount of water (100 μL) and then irradiated by a NIR laser (808 nm; 0.75 W cm$^{-2}$). The temperature of these patterned films was measured using a thermal imaging camera (emissivity: 0.95) and the thermograms are shown in Fig. 1b and Fig. S2 of ESI.† The maximum temperature in the patterned region was determined and plotted as a function of irradiation time in Fig. 1c. These results show that irradiation of the patterned catechol resulted in a more rapid increase in temperature (*vs.* the control unpatterned film). Further, Fig. 1c shows that patterned films fabricated with increasing amounts of catechol (*i.e.*, higher $Q_{fab}$) show higher asymptotic temperatures. The effect of catechol modification on the film's photothermal properties is summarized in Fig. 1d. In summary, these initial studies indicate that catechol confers photothermal properties to chitosan hydrogels.

In a second experiment, we electrofabricated catechol-modified chitosan films using the two steps illustrated in Fig. 2a. In this case, a chitosan film was first deposited on the transparent circular gold electrode (4 mm diameter) by immersing the electrode in a chitosan solution (1.5 w/v%; pH 5.5) and imposing a cathodic voltage (−1.0 V *vs.* Ag|AgCl for 15 minutes). Next the

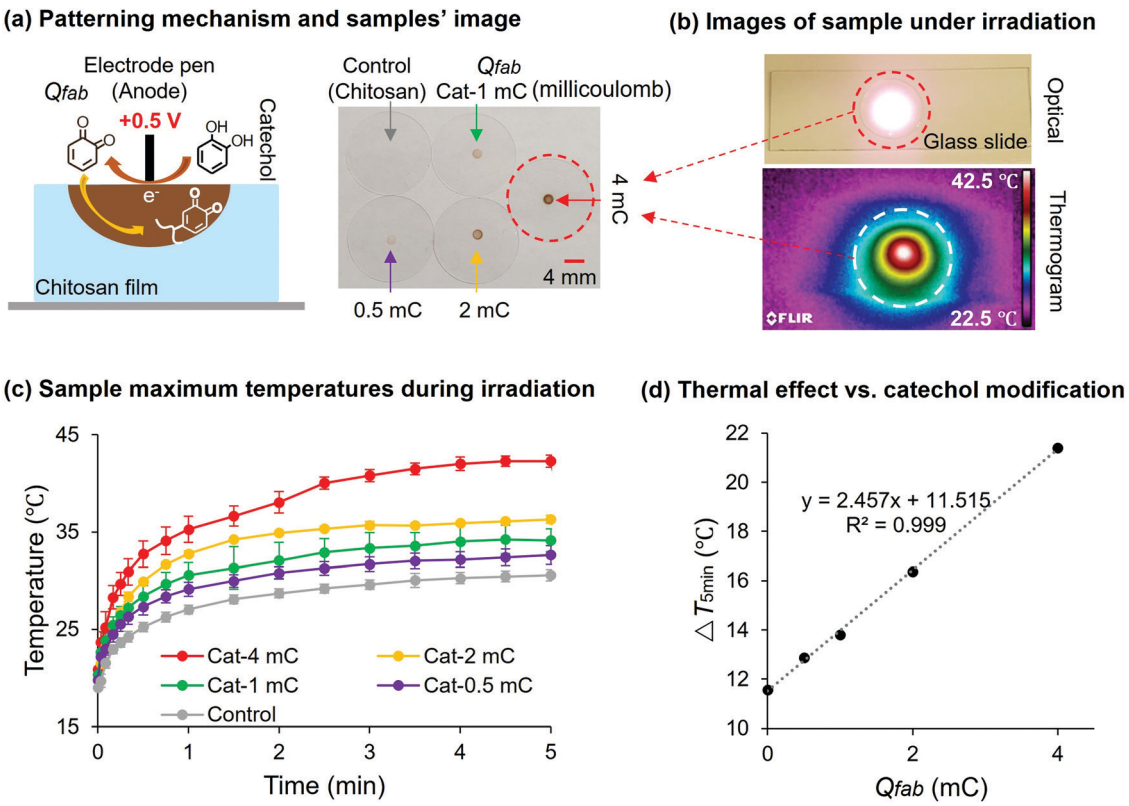


Fig. 1 Photothermal properties of patterned catechol films. (a) Catechol dots (2 mm diameter) were electrochemically 'written' onto cast chitosan films. (b) The temperature during NIR irradiation was determined by thermal imaging. (c) The increase of temperature (measured as maximum temperature) of the patterned regions during laser irradiation (808 nm; 0.75 W cm$^{-2}$; data represent mean values ± SD ($n$ = 3)). (d) Patterned catechols show a thermal effect which is linearly correlated to the catechol modification where $\Delta T_{5min}$ is the temperature difference between 0 and 5 min. [Note: "mC" is an abbreviation for millicoulomb.].

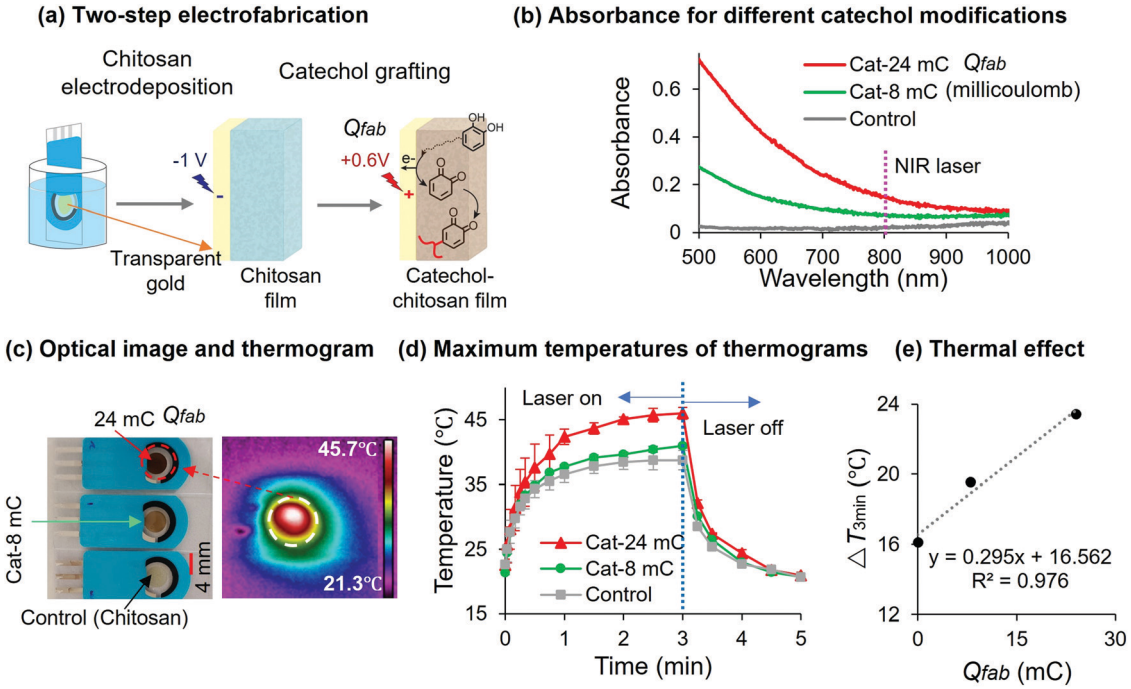


Fig. 2 Photothermal properties of catechol-chitosan coated electrodes. (a) Catechol-chitosan films are electrofabricated on transparent gold electrodes (4 mm diameter). (b) UV-Vis spectra of coated-electrodes with different extents of catechol modification (spectra were corrected from the blank signal of uncoated electrode). (c) Optical images and thermogram of film-coated electrode. (d) Maximum temperatures of the coated electrodes (808 nm laser; 0.75 W $cm^{-2}$; data represent mean values ± SD ($n$ = 3)). (e) Catechol coatings show a thermal effect which is quasi-linearly correlated to extent of catechol modification ($\Delta T_{3min}$ is the temperature difference between 0 and 3 min). [Note: "mC" is an abbreviation for millicoulomb.].

chitosan-coated electrode was immersed in a catechol solution (10 mM) and an anodic voltage was applied (+0.6 V *vs.* Ag|AgCl for varying times up to 3 minutes). These film-coated electrodes were rinsed, immersed in phosphate buffer, and the UV-Vis-NIR spectra was collected. Fig. 2b shows a featureless, broad-band absorbance that extends into the NIR region. In addition, Fig. 2b shows higher UV-Vis-NIR absorption for the film fabricated with a higher extent of catechol modification.

These electrofabricated films were then dried in air, wet with a small amount of water (50 μL), and irradiated by a NIR laser (808 nm; 0.75 W $cm^{-2}$). The temperature of the irradiated film-coated electrodes was measured using the IR camera and the thermograms are shown in Fig. 2c and Fig. S3 of ESI.† Temperature-time plots in Fig. 2d show a temperature rise for the control chitosan-coated gold electrode which is consistent with photothermal properties of this electrode's gold and carbon regions (note: the concentric carbon black rings that are visible in the electrodes of Fig. 2c are typically used as counter electrodes, but were not used in our study).[33] Nevertheless, electrodes coated with catechol-chitosan films show a larger increase in temperature and this increase was greater for films fabricated with higher extents of catechol modification. The summary plot in Fig. 2e shows the correlation between the temperature rise ($\Delta T$) and catechol modification ($Q_{fab}$), and these results further demonstrate the photothermal properties of the catechol-chitosan films.

The top-down experimental method to measure redox-activities is illustrated in Fig. 3a, which shows how two mediators and an oscillating voltage are imposed to sequentially exchange electrons with the grafted catechol moieties. The $Ru(NH_3)_6Cl_3$ ($Ru^{3+}$) mediator transfers electrons from the electrode to the film by a reductive redox-cycling mechanism, while the ferrocene dimethanol (Fc) mediator transfers electrons from the film to the electrode by an oxidative redox-cycling mechanism (note: the quinone and catechol moieties in Fig. 3a suggest putative oxidized and reduced molecular structures although the underlying chemistry may be more complex and heterogeneous). Fig. 3b shows cyclic voltammograms of catechol (24 mC)-chitosan coated electrode in 0.1 M phosphate buffer with and without mediators (1 mM $Ru^{3+}$ and 1 mM Fc). In the absence of mediators, negligible currents are observed indicating the catechol-chitosan films are non-conducting. In the presence of the two mediators, amplified and partially-rectified currents are observed which is explained by redox-cycling of the two mediators between the electrode and film's catechol moieties. These results demonstrate that catechol films are redox active but non-conducting.

To simultaneously impose both redox and NIR stimuli, Fig. 3c shows we irradiated the electrode during redox-probing time-series measurements. Data from these redox-probing studies can be represented as time-series of input voltages and output currents. The data for the first 5 redox-probing cycles in Fig. 3d illustrate such time-series data in the absence of irradiation (laser off). The amplified currents for the electrode coated with the catechol-chitosan film (*vs.* control electrode coated with only chitosan) provide evidence that the catechol-coated electrodes possess redox-activity. The apparent

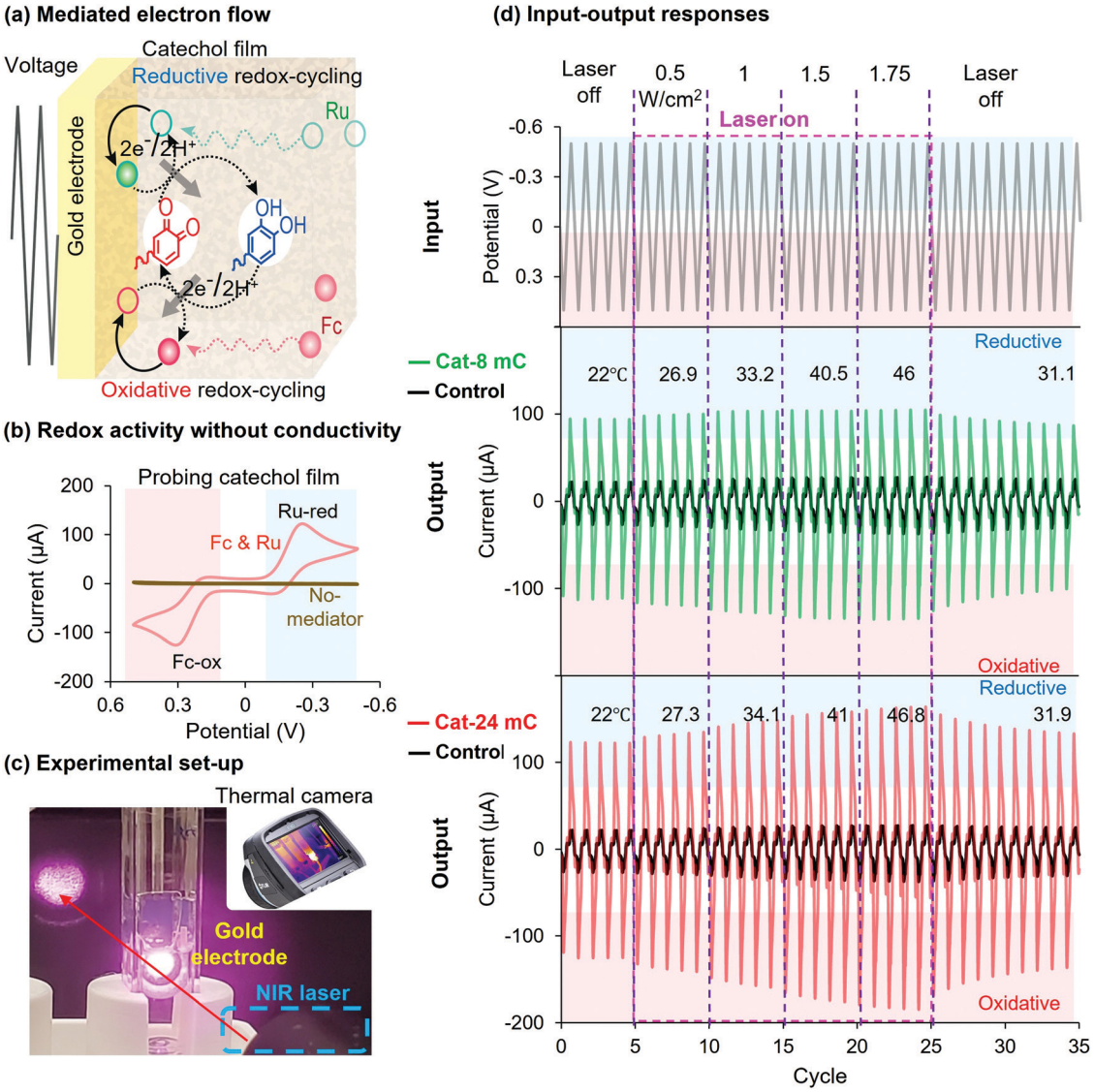


Fig. 3 Simultaneous stimulation of films by redox-probing and NIR irradiation. (a) Catechol films are redox-active as evidenced by their ability to undergo redox-cycling reactions with the diffusible mediators $Ru(NH_3)_6Cl_3$ ($Ru^{3+}$) and ferrocene dimethanol (Fc). (b) Cyclic voltammograms for the catechol (24 mC)-chitosan coated electrode show the film is redox active but non-conducting. (c) Experimental approach to simultaneously stimulate film-coated electrodes with redox inputs and NIR irradiation (outputs monitored electrochemically and by a thermal imaging camera). (d) Times-series data show the imposed voltage input and observed output current responses: the amplified peak currents for the catechol-chitosan (*vs.* chitosan) films provides evidence of redox-activity; the steady output response provides evidence that the redox-activities are reversible; and the small change in output currents upon NIR irradiation provides initial evidence that the responses to redox and NIR inputs can be independent.

steady (*i.e.*, time-invariant) output currents provide evidence that the catechol moieties are reversibly redox-active and can be repeatedly oxidized and reduced through redox-cycling. Comparison of the bottom two output current plots show that films fabricated with higher extents of catechol modification have larger peak currents which is consistent with the expectation that redox activities are correlated to the extent of catechol modification.

To detect interactions between redox and NIR stimulation, we simultaneously irradiated the catechol-coated electrode while redox-probing with an imposed oscillating input voltage. As illustrated in Fig. 3d, we started by redox-probing in the absence of NIR irradiation and after 5 cycles we began irradiation with 808 nm laser at a power density of 0.5 W $cm^{-2}$. The results in the bottom two plots show a gradual increase in output currents during these 5 cycles and the temperatures listed above the output curves were measured during the 4th cycle for the catechol-chitosan coated electrodes. This procedure of increasing irradiation power measuring output currents for 5 cycles and measuring temperature was repeated for three additional powers (1, 1.5 and 1.75 W $cm^{-2}$). In each case, both the oxidative and reductive output currents increased. Finally, we turned off the laser and redox-probed the film for an additional 10 cycles and observed both the output currents and temperature (measured during the 9th cycle) returned toward the pre-irradiation values. [Notes: (i) these results show reversibility in the short-term while

 

long-term stability tests were not performed; and (ii) Fig. S4 of the ESI† shows analysis of the time-series charge $(Q = \int i\mathrm{d}t)$ which often provides a more sensitive means to detect subtle changes in output response.] Overall, the results in Fig. 3d indicate that NIR irradiation has a comparatively small effect on the catechol-films' redox-activities and this effect is reversible (*i.e.*, the redox activity is nearly the same before and after irradiation). Potentially, the small enhancement in output currents observed upon irradiation could be the result of thermal heating (and not photo-induced electron transfer).

In addition to representing time-series data as input-output curves, it is common to represent such systems-level measurements as phase-plane plots where time is not explicitly shown. Such phase-plane plots in electrochemistry are cyclic voltammograms (CVs). Fig. 4a shows the CV-representation for the data from the 4th cycle for each of the 5-cycle redox-probing tests at different irradiation powers for a catechol-chitosan coated electrode (Cat-24 mC). [Summaries of the data for electrodes coated with the control chitosan and catechol-chitosan (Cat-8 mC) films are provided in Fig. S5 of ESI†]. These CV waveforms show higher peak currents (*i*pa and *i*pc) upon NIR-irradiation and the peak currents were higher with higher irradiation powers. Further, these CVs show the voltage difference between peak currents ($\Delta E$) becomes somewhat smaller when the films were irradiated with higher powers. Otherwise, the waveforms do not show qualitative changes that might be expected if NIR irradiation induced new electron transfer processes. Potentially, the observed quantitative changes in waveform may have resulted from thermal heating effects on physicochemical processes (*e.g.*, mediator diffusion) unrelated to photo-induced electron transfer.

To investigate the thermal effects, we performed equivalent redox-probing "control" measurements at different temperatures. Specifically, the electrochemical cell was placed in an incubator at

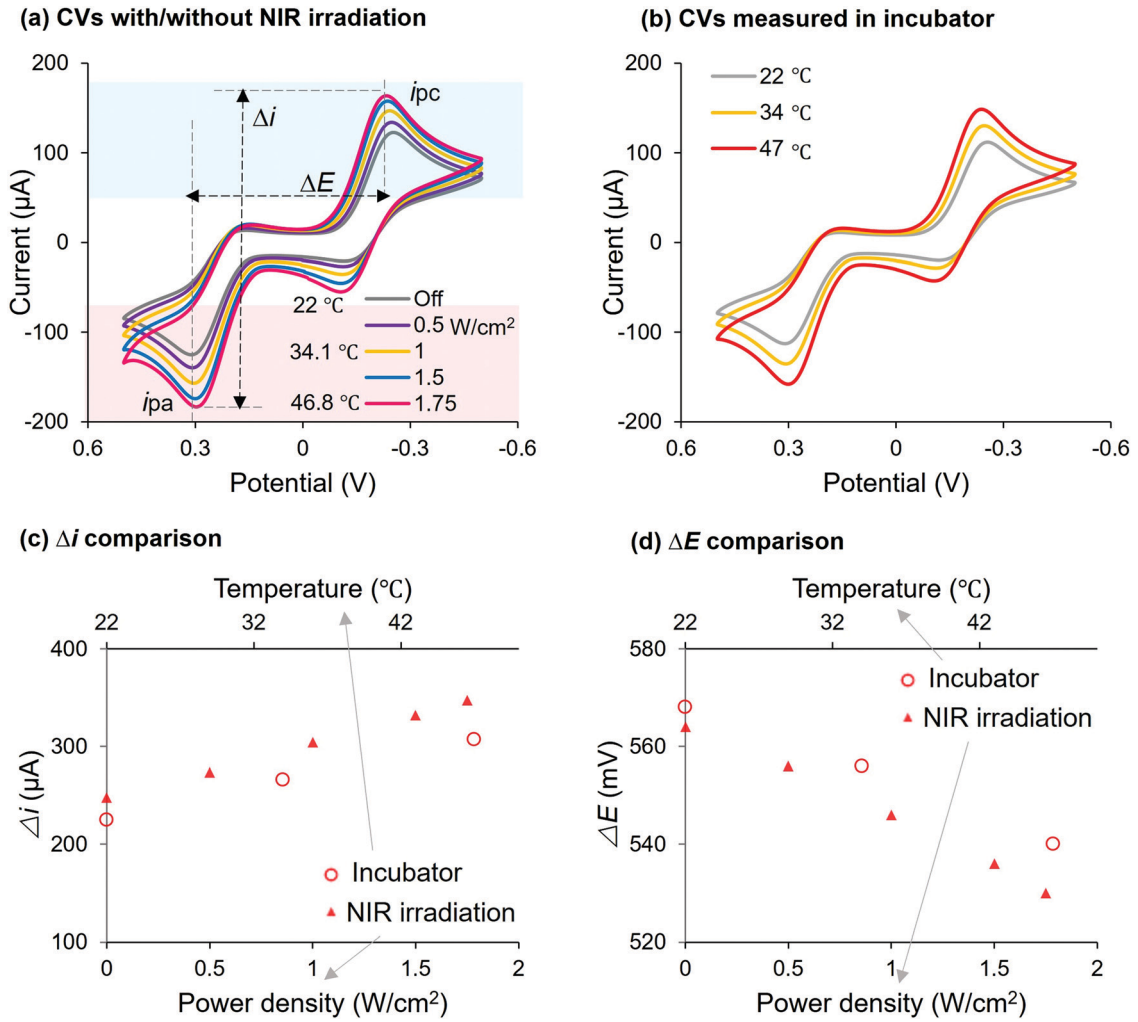


Fig. 4 Cyclic voltammogram (CV) analysis that suggests the observed effects of NIR-irradiation may be due to photothermal heating. (a) Measurements for catechol (24 mC)-chitosan coated electrode that was simultaneously stimulated by redox-probing and NIR-irradiation (same data as in Fig. 3d). (b) Measurements for the same film that was stimulated by redox-probing at elevated temperatures (without NIR-irradiation). (c) Both experiments show large and similar increases in current amplitude $\Delta i$ for the film that was NIR-irradiated or heated. (d) Both experiments show small and similar decreases in $\Delta E$ for the film that was NIR-irradiated or heated.

three different temperatures (22, 34 and 47 °C) that correspond to those measured from the photothermal heating in Fig. 3d for catechol-chitosan coated electrode (Cat-24 mC). We acknowledge that these constant-temperature redox-probing experiments are approximate controls: while they allow probing at the same bulk temperatures observed during NIR-irradiation experiments, they cannot recapitulate the spatial and temporal temperature gradients that occur during photothermal heating. The CV waveforms in Fig. 4b show the same qualitative features as those in Fig. 4a, while the quantitative features (*i.e.*, larger peak currents or current amplitude $\Delta i$, and smaller $\Delta E$ values for measurements at higher temperatures) are also similar to those in Fig. 4a. Overall, the results from these control experiments suggest that the increased currents observed in Fig. 4a may be mostly due to photothermal heating and not photochemically-induced electron transfer reactions.

Fig. 4c and d summarize the quantitative changes in peak currents (or $\Delta i$) and $\Delta E$ values respectively, for the experiments from Fig. 4a (simultaneous redox-probing and NIR-irradiation) and Fig. 4b (redox-probing at elevated temperatures). As discussed, the current amplitude $\Delta i$ increases and the $\Delta E$ decreases with either NIR-irradiation or thermal heating. As shown, both the magnitudes and trends for these changes in $\Delta i$ and $\Delta E$ were similar between the two experiments which further suggests the observed changes upon NIR-irradiation may be due to thermal heating on physicochemical processes (*e.g.*, mediator diffusion[34]). In summary, the observed changes in the redox-activities of the catechol-modified chitosan films upon NIR irradiation are reversible and appear to be primarily the result of reversible photothermal heating (and not photo-induced electron transfer).

# Conclusions

In conclusion, our top-down property measurements indicate that catechol-chitosan films are photothermally active, and that their response to NIR stimuli is reversible and largely independent of the reversible responses to redox inputs. From a fundamental perspective, this result suggests that energy (and information) can "flow" through catecholic materials *via* independent molecularly-based redox modality and electromagnetically-based optical modality. However, there are three important caveats when using these top-down property measurements to provide bottom-up (molecular level) mechanistic explanations. First, it is possible that our electrochemical measurements are insufficiently sensitive to detect opto-redox coupling between NIR-induced electron-excitation and mediator-induced electron-transfer. Second, it is possible that opto-redox coupling is not observed under the conditions used simply because NIR irradiation likely leads to modest excitation and redox-probing with dilute mediators may limit interactions with an excited state. Finally, it is possible that the observed opto-redox independence is the result of chemical heterogeneities within the catechol-grafted film: specifically, it is possible that the moieties responsible for photoexcitation are distinct and separated from the moieties responsible for redox activities.

We envision that the practical implications of this work are for redox-based bioelectronics. As mentioned, catechols are emerging as important circuit elements because they possess various molecular electronic properties. In particular, redox-active catechol materials can amplify, rectify, and gate redox-based currents[6,7] as well as serve as molecular memory devices.[29,35] As illustrated in Fig. 1a, such catechols can be patterned onto flexible and sustainable polysaccharide matrices: the pattern of the covalently-grafted catechols serve as a permanent memory while the redox-activity of the patterned catechol serves as a "volatile" two-state (oxidized and reduced) short-term memory. Previous studies showed that this short-term memory can be "read" optically based on catechol's redox-state-dependent absorbance in the visible region (480 nm),[29] and this optical reading enables convenient cell-phone imaging to access biologically-relevant redox-based chemical information.[36] The results from the current study indicate that the long term memory (*i.e.*, the pattern) can also be read optically and non-destructively using radiation from a different region of the electromagnetic spectrum (808 nm). In addition to reading (*i.e.*, sensing), we envision that catechol's photothermal properties could provide a simple means for actuation just as its redox properties have been used for biological actuation.[11,37] Overall, we believe these results expand the molecular electronic properties of catechol-based materials to enable communication through both short-range redox modalities and long-range electromagnetic modalities.

# Materials and methods

### Materials

Chitosan, hydrochloric acid, sodium hydroxide, catechol, $Ru(NH_3)_6Cl_3$ and 1,1-ferrocene dimethanol were purchased from Sigma-Aldrich. All reagents were used as received without further purification. All solutions were prepared using Millipore water (>18 MΩ). The solution of mediators (1 mM $Ru(NH_3)_6Cl_3$ and 1 mM 1,1-Ferrocenedimethanol) was prepared in 0.1 M phosphate buffer (pH 7.0).

### Instrumentation

The electrochemical cell consisted of a counter electrode made of 0.3 mm platinum wire, a Ag|AgCl reference electrode, and a screen-printed gold transparent (4 mm diameter; from Metrohm) working electrode. All electrochemical measurements and electrofabrication were carried out using potentiostat (CHI 760E, CH Instruments). Infrared diode laser at 808 nm (MDL-N-808, CNI Lasers) was used for the irradiation experiments. Laser power meter (FieldMate, Coherent) was used for the laser irradiation calibration, with the power density normalized by the surface area of laser spot. Thermal imaging camera (FLIR E40, Teledyne FLIR) was used for the temperature measurements in NIR irradiation experiments. Cell-phone (Galaxy S10, Samsung) camera was used for optical imaging. Incubator (Classic C24, New Brunswick) was used for the elevated temperature experiments with temperature calibrated by a mercury thermometer. The UV-Vis-NIR absorption was collected using a spectrophotometer (Evolution 60, Thermo Scientific).

 

### Patterning of catechol on chitosan film

A chitosan solution (1.5% w/v) was prepared by dissolving chitosan with 1 M hydrochloric acid until final pH 5.5. This chitosan solution (100 μL) was cast onto a microscope circular cover glass (18 mm diameter) and left to dry overnight. The dried film was neutralized by immersing in a 1 M sodium hydroxide solution for 1 hour and rinsed thoroughly with water to form a hydrogel film. This chitosan film (with glass) was then immersed in a 10 mM catechol solution (in 0.1 M phosphate buffer, pH 7.0), and a standard gold electrode (2 mm diameter) was directly placed above the film for catechol patterning as illustrated in Fig. 1a. An anodic potential (0.5 V *vs.* Ag|AgCl) was applied to the gold electrode until a desired (0.5, 1, 2 and 4 mC) charge was achieved.

### Electro-fabrication of catechol film

The two electro-fabrication steps were both carried out using the three-electrode system (transparent gold working electrode) as illustrated in Fig. 2a. The electrodes were immersed in the chitosan solution (1.5% w/v, pH 5.5), and a cathodic potential (−1.0 V *vs.* Ag|AgCl) was applied for 15 minutes to electrodeposit chitosan. Then, the chitosan hydrogel film coated electrode was removed from chitosan solution and rinsed with water. This electrode coated with the chitosan film served as an experimental control. To generate a catechol-chitosan film in the second step, the chitosan film coated electrode was immersed into a 10 mM catechol solution (in 0.1 M phosphate buffer), and an anodic potential (+0.6 V *vs.* Ag|AgCl) was applied to the electrode until a desired charge (8 or 24 mC) was achieved.

## Author contributions

Zhiling Zhao: conceptualization, investigation, data curation, visualization and writing. Eunkyoung Kim: conceptualization and investigation. Chen-Yu Chen, John R. Rzasa, Qian Zhang and Yang Tao: resources. Jinyang Li: methodology. William E. Bentley, Jean-Philip Lumb and Bern Kohler: conceptualization. Gregory F. Payne: conceptualization, supervision, funding acquisition and writing.

## Conflicts of interest

There are no conflicts of interest to declare.

## Acknowledgements

This work was supported by the National Science Foundation (CBET #1932963), the Defense Threat Reduction Agency (HDTRA1-19-0021), and the Department of Energy, OBER, Lawrence Livermore National Laboratory SFA (under Contract DE-AC52-07NA27344, LLNL-JRNL-827946).

## References

1 M. D'Ischia, A. Napolitano, A. Pezzella, P. Meredith and M. Buehler, Melanin Biopolymers: Tailoring Chemical Complexity for Materials Design, *Angew. Chem.*, 2020, **132**(28), 11292–11301, DOI: **10.1002/ange.201914276**.

2 H. Lee, S. M. Dellatore, W. M. Miller and P. B. Messersmith, Mussel-Inspired Surface Chemistry for Multifunctional Coatings, *Science*, 2007, **318**(5849), 426–430.

3 H. A. Lee, E. Park and H. Lee, Polydopamine and Its Derivative Surface Chemistry in Material Science: A Focused Review for Studies at KAIST, *Adv. Mater.*, 2020, **32**(35), 1907505.

4 K. Lee, M. Park, K. G. Malollari, J. Shin, S. M. Winkler, Y. Zheng, J. H. Park, C. P. Grigoropoulos and P. B. Messersmith, Laser-Induced Graphitization of Polydopamine Leads to Enhanced Mechanical Performance While Preserving Multifunctionality, *Nat. Commun.*, 2020, **11**(1), 1–8.

5 E. Kim, Y. Liu, X. W. Shi, X. Yang, W. E. Bentley and G. F. Payne, Biomimetic Approach to Confer Redox Activity to Thin Chitosan Films, *Adv. Funct. Mater.*, 2010, **20**(16), 2683–2694, DOI: **10.1002/adfm.200902428**.

6 E. Kim, W. T. Leverage, Y. Liu, I. M. White, W. E. Bentley and G. F. Payne, Redox-Capacitor to Connect Electrochemistry to Redox-Biology, *Analyst*, 2014, **139**(1), 32–43, DOI: **10.1039/c3an01632c**.

7 S. Wu, E. Kim, J. Li, W. E. Bentley, X.-W. Shi and G. F. Payne, Catechol-Based Capacitor for Redox-Linked Bioelectronics, *ACS Appl. Electron. Mater.*, 2019, **1**(8), 1337–1347, DOI: **10.1021/acsaelm.9b00272**.

8 X. Zhou, N. C. McCallum, Z. Hu, W. Cao, K. Gnanasekaran, Y. Feng, J. F. Stoddart, Z. Wang and N. C. Gianneschi, Artificial Allomelanin Nanoparticles, *ACS Nano*, 2019, **13**(10), 10980–10990.

9 W. Cao, A. J. Mantanona, H. Mao, N. C. McCallum, Y. Jiao, C. Battistella, V. Caponetti, N. Zang, M. P. Thompson and M. Montalti, Radical-Enriched Artificial Melanin, *Chem. Mater.*, 2020, **32**(13), 5759–5767.

10 E. Kim, Y. Liu, C. J. Baker, R. Owens, S. Xiao, W. E. Bentley and G. F. Payne, Redox-Cycling and H 2 O 2 Generation by Fabricated Catecholic Films in the Absence of Enzymes, *Biomacromolecules*, 2011, **12**(4), 880–888, DOI: **10.1021/bm101499a**.

11 J. Li, S. P. Wang, G. Zong, E. Kim, C.-Y. Tsao, E. VanArsdale, L. X. Wang, W. E. Bentley and G. F. Payne, Interactive Materials for Bidirectional Redox-Based Communication, *Adv. Mater.*, 2021, **33**(18), 2007758.

12 T. R. Eliato, J. T. Smith, Z. Tian, E.-S. Kim, W. Hwang, C. P. Andam and Y. J. Kim, Melanin Pigments Extracted from Horsehair as Antibacterial Agents, *J. Mater. Chem. B*, 2021, **9**(6), 1536–1545.

13 Y. Li, R. Fu, Z. Duan, C. Zhu and D. Fan, Mussel-Inspired Adhesive Bilayer Hydrogels for Bacteria-Infected Wound Healing via NIR-Enhanced Nanozyme Therapy, *Colloids Surf., B*, 2022, **210**, 112230.

14 E. Kim, M. Kang, T. Tschirhart, M. Malo, E. Dadachova, G. Cao, J. J. Yin, W. E. Bentley, Z. Wang and G. F. Payne, Spectroelectrochemical Reverse Engineering DemonstratesThat Melanin's Redox and Radical Scavenging Activities Are Linked, *Biomacromolecules*, 2017, **18**(12), 4084–4098, DOI: **10.1021/acs.biomac.7b01166**.

15 C. Cao, E. Kim, Y. Liu, M. Kang, J. Li, J.-J. Yin, H. Liu, X. Qu, C. Liu, E. W. Bentley and G. F. Payne, Radical Scavenging Activities of Biomimetic Catechol-Chitosan Films, *Biomacromolecules*, 2018, **19**(8), 3502–3514, DOI: **10.1021/acs.biomac.8b00809**.

16 H. Liu, X. Qu, H. Tan, J. Song, M. Lei, E. Kim, G. F. Payne and C. Liu, Role of Polydopamine's Redox-Activity on Its pro-Oxidant, Radical-Scavenging, and Antimicrobial Activities, *Acta Biomater.*, 2019, **88**, 181–196, DOI: **10.1016/j.actbio.2019.02.032**.

17 I. S. Kwon and C. J. Bettinger, Polydopamine Nanostructures as Biomaterials for Medical Applications, *J. Mater. Chem. B*, 2018, **6**(43), 6895–6903.

18 Y. J. Kim, A. Khetan, W. Wu, S. Chun, V. Viswanathan, J. F. Whitacre and C. J. Bettinger, Evidence of Porphyrin-Like Structures in Natural Melanin Pigments Using Electrochemical Fingerprinting, *Adv. Mater.*, 2016, **28**(16), 3173–3180.

19 C. Grieco, F. R. Kohl, A. T. Hanes and B. Kohler, Probing the Heterogeneous Structure of Eumelanin Using Ultrafast Vibrational Fingerprinting, *Nat. Commun.*, 2020, **11**(1), 1–9, DOI: **10.1038/s41467-020-18393-w**.

20 S. Takeuchi, W. Zhang, K. Wakamatsu, S. Ito, V. J. Hearing, K. H. Kraemer and D. E. Brash, Melanin Acts as a Potent UVB Photosensitizer to Cause an Atypical Mode of Cell Death in Murine Skin, *Proc. Natl. Acad. Sci. U. S. A.*, 2004, **101**(42), 15076–15081, DOI: **10.1073/pnas.0403994101**.

21 D. E. Brash, UV-Induced Melanin Chemiexcitation: A New Mode of Melanoma Pathogenesis, *Toxicol. Pathol.*, 2016, **44**(4), 552–554.

22 J. Song, H. Liu, M. Lei, H. Tan, Z. Chen, A. Antoshin, G. F. Payne, X. Qu and C. Liu, Redox-Channeling Polydopamine-Ferrocene (PDA-Fc) Coating to Confer Context-Dependent and Photothermal Antimicrobial Activities, *ACS Appl. Mater. Interfaces*, 2020, **12**(7), 8915–8928, DOI: **10.1021/acsami.9b22339**.

23 X. Xie, Z. Wang, M. Zhou, Y. Xing, Y. Chen, J. Huang, K. Cai and J. Zhang, Redox Host–Guest Nanosensors Installed with DNA Gatekeepers for Immobilization-Free and Ratiometric Electrochemical Detection of MiRNA, *Small Methods*, 2021, **5**(12), 2101072.

24 X. Zhang, Y. Peng, X. Wang and R. Ran, Melanin-Inspired Conductive Hydrogel Sensors with Ultrahigh Stretchable, Self-Healing, and Photothermal Capacities, *ACS Appl. Polym. Mater.*, 2021, **3**(4), 1899–1911, DOI: **10.1021/acsapm.0c01430**.

25 S. Sakib, F. Bakhshandeh, S. Saha, L. Soleymani and I. Zhitomirsky, Surface Functionalization of Metal Oxide Semiconductors with Catechol Ligands for Enhancing Their Photoactivity, *Sol. RRL*, 2021, **5**(10), 2100512.

26 T. Ding, Z. Wang, D. Xia, J. Zhu, J. Huang, Y. Xing, S. Wang, Y. Chen, J. Zhang and K. Cai, Long-Lasting Reactive Oxygen Species Generation by Porous Redox Mediator-Potentiated Nanoreactor for Effective Tumor Therapy, *Adv. Funct. Mater.*, 2021, **31**(13), 2008573.

27 R. Micillo, L. Panzella, M. Iacomino, G. Prampolini, I. Cacelli, A. Ferretti, O. Crescenzi, K. Koike, A. Napolitano and M. d'Ischia, Eumelanin Broadband Absorption Develops from Aggregation-Modulated Chromophore Interactions under Structural and Redox Control, *Sci. Rep.*, 2017, **7**(1), 1–12.

28 W. Xie, E. Pakdel, Y. Liang, Y. J. Kim, D. Liu, L. Sun and X. Wang, Natural Eumelanin and Its Derivatives as Multifunctional Materials for Bioinspired Applications: A Review, *Biomacromolecules*, 2019, **20**(12), 4312–4331.

29 S. Wu, E. Kim, C. Chen, J. Li, E. VanArsdale, C. Grieco, B. Kohler, W. E. Bentley, X. Shi and G. F. Payne, Catechol-Based Molecular Memory Film for Redox Linked Bioelectronics, *Adv. Electron. Mater.*, 2020, **6**(10), 2000452.

30 K. Rorabeck and I. Zhitomirsky, Dispersant Molecules with Functional Catechol Groups for Supercapacitor Fabrication, *Molecules*, 2021, **26**(6), 1709.

31 L. Q. Wu, M. K. McDermott, C. Zhu, R. Ghodssi and G. F. Payne, Mimicking Biological Phenol Reaction Cascades to Confer Mechanical Function, *Adv. Funct. Mater.*, 2006, **16**(15), 1967–1974.

32 L. Q. Wu, R. Ghodssi, Y. A. Elabd and G. F. Payne, Biomimetic Pattern Transfer, *Adv. Funct. Mater.*, 2005, **15**(2), 189–195, DOI: **10.1002/adfm.200400279**.

33 X. Wu, G. Y. Chen, G. Owens, D. Chu and H. Xu, Photothermal Materials: A Key Platform Enabling Highly Efficient Water Evaporation Driven by Solar Energy, *Mater. Today Energy*, 2019, **12**, 277–296.

34 A. Boika and A. S. Baranski, Dielectrophoretic and Electrothermal Effects at Alternating Current Heated Disk Microelectrodes, *Anal. Chem.*, 2008, **80**(19), 7392–7400.

35 S. Wu, Z. Zhao, J. R. Rzasa, E. Kim, J. Li, E. VanArsdale, W. E. Bentley, X. Shi and G. F. Payne, Hydrogel Patterning with Catechol Enables Networked Electron Flow, *Adv. Funct. Mater.*, 2021, **31**(11), 2007709.

36 S. Wu, J. R. Rzasa, E. Kim, Z. Zhao, J. Li, W. E. Bentley, N. N. Payne, X. Shi and G. F. Payne, Catechol Patterned Film Enables the Enzymatic Detection of Glucose with Cell Phone Imaging, *ACS Sustainable Chem. Eng.*, 2021, **9**(44), 14836–14845.

37 H. Liu, X. Qu, E. Kim, M. Lei, K. Dai, X. Tan, M. Xu, J. Li, Y. Liu, X. Shi, P. Li, G. F. Payne and C. Liu, Bio-Inspired Redox-Cycling Antimicrobial Film for Sustained Generation of Reactive Oxygen Species, *Biomaterials*, 2018, **162**, 109–122, DOI: **10.1016/j.biomaterials.2017.12.027**.

 